Synthesis and properties of mercury selenide colloidal quantum dots

© N.D. Zhukov[1], O.Yu. Tsvetkova[1], M.V. Gavrikov[1,2], A.G. Rokakh[2], T.D. Smirnova[3], S.N. Shtykov[3]

[1] OOO NPP „Volga“,
410033 Saratov, Russia
[2] Institute of Physics in Saratov State University,
410012 Saratov, Russia
[3] Institute of Chemistry in Saratov State University,
410012 Saratov, Russia

E-mail: ndzhukov@rambler.ru

Received December 1, 2021
Revised December 23, 2021
Accepted December 27, 2021

Colloidal nanocrystals (quantum dots (QDs)) of mercury selenide have been synthesized and the effect of size quantization on their basic properties has been investigated. The current-voltage characteristics of single QDs (less than 10 nm) had features in the form of separate regular peaks and quasi-periodic current oscillations with voltage intervals (0.1−0.2) V. The observed features were explained in the models of size quantization and Bloch oscillations. The absorption spectra in the range up to 25 μm had eight certain peaks, including five — interband and intraband transitions and three — with energies (145−215) meV, which are explained as intraresonant. Calculations show that it is possible to have IR photosensitivity in the wavelength range up to 40 μm.

Keywords: Colloidal synthesis, nanocrystal, quantum dot, mercury selenide, dimensional quantization, Bloch pulsations, electron transport, IR absorption, IR photosensitivity.

DOI: 10.21883/SC.2022.04.54315.9779

1. Introduction

The colloidal quantum dots (QD) are nanosized semiconductor crystals, the surface of which is coated with ligands, which make them stable in aqueous or non-aqueous solutions. The properties of colloidal QDs can be controlled in the course of their synthesis, for that reason thousands of works are devoted to the conditions for their preparation, methods for controlling the structure and sizes, surface modification, and applications in various fields [1,2]. The synthesis of QD based on relatively wide-gap semiconductor chalcogenides of cadmium, indium, zinc, and lead has been studied for almost three decades, and the conditions for their preparation are well known. Recently the increased attention is paid to the synthesis of semiconductor nanoparticles with an almost zero band gap (gapless semiconductors), which include mercury chalcogenides. Interband charge processes in such QDs allow to obtain the effects of photodetection and photoluminescence in the mid and far IR-spectrum region and even, theoretically, in the terahertz range, which significantly complements the QD spectral range in relation to those based on cadmium compounds and allows to create new optoelectronic devices [3,4].

The time delay in obtaining mercury chalcogenides compared, for example, to cadmium chalcogenides, is caused by a number of factors, among them — increased toxicity of mercury precursors and IR-luminescence range, which is not very convenient for researchers due to inaccessible equipment, as well as lack of demand for such QDs in medicine [5]. With the development of technology, these problems were partially solved, but new ones added to them, in particular, — difficulties in achieving the required parameters of photo registration and photoluminescence [3–5]. To obtain effects in the far IR-spectrum, nanocrystals of comparatively large sizes — up to 30 nm are required. It was shown in the study [3], that QDs of such sizes have a polycrystalline structure, that reduces the manifestation of luminescence and photoconductivity effects. In our study [6] we made a reasonable assumption, that during colloidal synthesis, the formation of the size of a nanocrystal with a perfect structure is limited by the ratio of its surface energy and van der Waals energy. Estimates show, that, perhaps, the limiting size of a perfect nanocrystal of mercury chalcogenides can be 5−6 nm. In this regard, the solution of problems should be sought in the way of studying small QDs and their inherent dimensional quantization effects.

The number of studies on the synthesis and properties of mercury selenide is extremely small, even in comparison with its sulfide and telluride. The conditions for obtaining mercury selenide in these studies often differs greatly, and each author investigates the properties, which are of interest for him. Thus, both the expansion of the methods and conditions of synthesis, and the range of obtained QDs properties remain an important task.

In our study we compared the previously described QD synthesis using mercury acetate [7] with the less toxic mercury oxide proposed by us as a precursor, and showed, that the obtained QDs have similar characteristics. The use of a poorly soluble oxide, in our opinion, also has a second advantage associated with the possibility of dosing the concentration of the resulting mercury oleate,

i.e. effects on the rate of QD nucleation and crystal growth. The obtained QDs were characterized according to the traditional methodology, in particular, TEM-images of transmission electron microscopy, optical absorption spectra, and X-ray analysis results confirming the chemical composition and stoichiometry of nanocrystals. The other side of the research task is to study the electron transport in the synthesized QDs, which allowed to obtain a number of new interesting results related to the manifestation of dimensional quantization.

2. Colloidal synthesis

The complexity of colloidal synthesis lies in the large number of process determinants (degrees of freedom) — compositions and quality of solvents, compositions and methods for preparing precursors, a variety of technological modes. The results of the synthesis are nanoparticles with a large number of characteristics and parameters. In the literature, however, a massive material has been accumulated, sufficient to choose the optimal options for certain tasks [3–5,7–10]. Our main task is to study the influence of dimensional quantization on the quantum dots properties. Technologically, it requires the synthesis of nanocrystals of relatively small (no more than 10 nm) sizes with the maximum perfect crystalline structure.

In the most commonly used methods of colloidal synthesis of mercury selenide nanoparticles, oleic acid is used as a solvent, and the following precursors are used: mercury — mercury oleate obtained from mercury acetate; selenium — its solution in trioctylphosphine. The use of long-chain and coordinating oleylamine as a solvent is of great importance for the synthesis of HgSe nanocrystals with a minimum size dispersion [3]. The temperature (80−100°C) and time ($\sim$ 1 min) of the process become the main determining and variable parameters for obtaining the required QD quality and sizes. Taking into account all this, and also due to the preliminary development of the technology, we have chosen the following optimal synthesis option.

The selected norm of acetate or mercury oxide, 10 ml of oleic acid and 25 ml of oleylamine are placed in a 50 ml three-necked flask. At a temperature of 85°C, the process is carried out with intensive stirring for 1 h in an atmosphere of dry nitrogen. Then the temperature is lowered and at 80°C 1.6 ml 1 M solution of selenium in trioctylphosphine is quickly introduced into the flask. After 1 min the reaction is stopped by placing the flask in cold water. The resulting darkish solution is then opened in air and the nanoparticles are precipitated by adding ethanol and centrifugation. The mother liquor is poured off, and the precipitate is dispersed in toluene. The cleaning procedure is repeated 2 more times. The last stage is selective precipitation to separate the batch into two or three fractions. To do this, the solution in pure toluene is first centrifuged without the addition of ethanol in order to get rid of the lamellar phase resulting from the complexation of mercury with oleylamine. In this case, only the stable solution is retained and the gray precipitate is discarded. A limited amount of ethanol is then added and the solution is centrifuged. The precipitate will become the second fraction, while the remaining particles in solution will be further precipitated by adding the selected amount of ethanol. The resulting fractions are then stored in a clean inert environment until they are used.

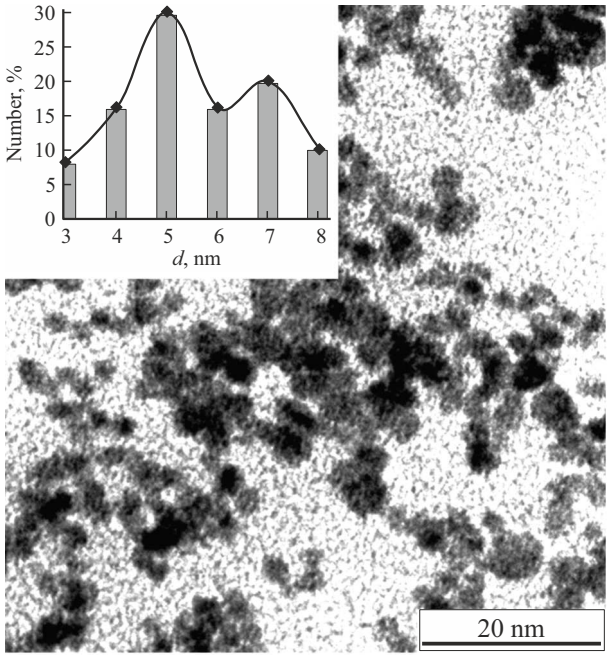

Figure 1. TEM-image of QD-HgSe layer fragment. On the insert — histogram and proportion distribution by size.

Figure 1 shows a typical fragmentary TEM-image of the QD-HgSe synthesized by us. TEM images were obtained with a transmission electron microscope Libra-120 (CarlZeiss, Germany). Comparative analysis showed the qualitative similarity of our images with similar ones in the literature [3].

The insert in Fig. 1 shows a histogram of the size distribution of our nanoparticles according to the data obtained from TEM-images on a random sample of five hundred nanoparticle dots from several batches of samples. Nanoparticle sizes were measured at high magnification on a monitor screen, by simple counting in rows of 20−30 replicas of nanoparticles in a row, with a total number of — at least 100 for each sample.

An important property of a nanocrystal is its crystalline structure, which is usually determined by X-ray diffraction analysis. However, there are practically no such studies in publications, which may be due to the difficulties in preparing samples suitable for the method [10]. Instead, the electron-X-ray microanalysis is usually carried out according to the X-ray pattern peaks, compared with reference data. In addition, the perfection of nanocrystals is indirectly assessed by their polygonal shape on high-resolution TEM-images and by light absorption properties determined on the basis

Table 1. X-ray microanalysis data

Element	Hg	Se	C	Si	O	Other	Total
Signal (abundance), %	23.8	9.1	39.8	21.9	4.9	0.5	100
Atomic weight	200	79	12	28	16		
Relative abundance, c.u.	8.4	8.6	0.3	1.3	3.2		21.8
Relative abundance, (c.u.), %	38.5	39.4	1.4	6.2	14.5		100

of optical measurements. The performed studies of the nanocrystals properties and comparisons with the literature data confirmed, that we have obtained nanocrystals of a perfect structure.

The elemental composition of nanoparticles was controlled by us by X-ray microanalysis using a Mira II LMU scanning electron microscope equipped with an energy-dispersive spectrometer system INCAEnergy 350 (TESCAN, Czech Republic). Just before the measurements the quantum dots were freed from the adsorbed on their surface ligands and antioxidant by separating the precipitate by centrifugation and redispersion in hexane, and they were deposited as islands on a silicon substrate in a thick layer, at least $10\,\mu$m.

Data on the chemical composition of the synthesized nanocrystals and its correspondence to calculations for the purpose of estimating the composition and stoichiometry are given in Table 1. The stoichiometric ratio of elements in QD was estimated by measuring the characteristic X-ray sensor signal as an indicator of relative abundance, which is proportional to the element atomic weight and the current in the exciting electronic beam and inversely proportional to the number of nanoparticles with which the electrons interact. As a characteristic of the number of atoms, we have chosen a certain conditional value proportional to the ratio of atomic mass to fractional content, — in Table 1 it is designated as „relative abundance". According to the data obtained (Table 1) and the chemical formula (HgSe), we can conclude, that QD composition corresponds to the desired stoichiometric ratio of elements, namely: $38.5:39.4 = 0.98:1$. A slight deviation from the exact equality of the elements is explained by the inevitable measurement and calculation error. Besides, it follows from Table 1 and X-ray patterns, that the oxygen detected by measurement is identified in the compounds with silicon and carbon (7.6 : 7.2), i.e. the synthesized HgSe compound does not contain oxidation traces.

It should be noted, that when using mercury compounds technologies, their toxicity, which is much higher for organic, rather than for inorganic compounds, is of great importance, (https://ru.wikipedia.org>wiki>Mercury). In this regard, we tested a method using mercury oxide instead of mercury acetate. Positive results were obtained for the main properties of quantum dots, but they require further technological optimization.

3. Dimensional quantization

The dimensional quantization properties in a quantum dot are defined by the processes of electron motion in it, which is described by the Schrödinger equation [11]. Solution of the equation exists only for a countable set of energy values $\tilde{E}_n$ and is a countable by quantum numbers n set of wave functions Ψ_n, which form a general solution as an additive superposition of particular solutions. For one-dimensional motion of an electron, the wave function Ψ_n of the discrete spectrum $\tilde{E}_n$ vanishes at finite values of the coordinate „x" n times (oscillatory theorem). These properties allow to simplify the problem of their study by reducing it to a particular one-dimensional linear case of motion at a distance x_0 and a rectangular potential V_0. Then one can obtain a particular solution of the Schrödinger equation in the form of $\Psi_n = 8mV_0(h^2n^2)^{-1}\sin(nx/x_0)$. De Broglie wavelength for an electron is then expressed by the formula $\Lambda \sim h(2m\tilde{E})^{-1/2} \sim 1.2(\tilde{E}m/m_0)^{-1/2}$, where $\tilde{E} = E_g + \tilde{E}_n$, and E_g – semiconductor band gap. Expressions for eigenfunctions $\tilde{E}_n$ can be obtained in the following form:

$$\tilde{E}_n \sim h^2n^2(8mx_0^2)^{-1} \sim 0.35n^2(a^2m/m_0)^{-1}, \qquad (1)$$

where h — Planck's constant, m — effective electron mass, m_0 — free electron mass, a — linear quantization size; $\tilde{E}_n$ and E_g — in electronvolts, Λ and a — in nanometers.

In a quantum dot, as a deep extended, a wide, potential well, the stable states of an electron are selected, so that an integer number of half-waves Ψ_n fit into the linear distance of its motion between the QD boundaries. Any affecting energy impact on an electron in the QD results in its transition from one steady state to another. The stability of state of an electron moving in a deep long potential well and the shape of its standing wave function may mean that its motion between the QD boundaries has a periodic resonant behavior.

QD sizes and the Brillouin zone properties, which are determined by the crystal structure expressed in the polygonal form of a nanocrystal, are of fundamental importance for the dimensional quantization process. QD-HgSe nanocrystals have a cubic syngony, and the simplest option of the resonant motion of an electron can be considered as a periodically oscillatory process between parallel planes of a right parallelepiped with a maximum distance between them, equal to one of the QD sizes. Dimensional

quantization is well manifested under a strong dimensional constraint, called confinement and is fulfilled at $a < \Lambda$.

The nature of electron motion under dimensional quantization conditions allows to assume, that a number of QD specific properties — its competition with the exciton mechanism during photoluminescence (PL), oscillations of the PL level and current in the current-voltage characteristic (CVC) are possible.

In our case, the photoluminescence of the obtained QD-HgSe was almost zero. We explain this by the small probability of formation and short lifetime of excitons, which are due to the supermobility of charge carriers in narrow-gap semiconductors, and by the fact, that dimensional quantization acts in QD-HgSe of small sizes, blocking the exciton mechanism. An analysis of the literature has shown that PL in QD-HgSe is actually observed only for wavelengths $> 3\,\mu$m, that corresponds to dimensions QD > 10 nm.

Our preliminary studies have shown that the photoluminescence of QD-HgSe, in contrast to standard photoluminophores, can experience enhancement when exposed to elevated temperature and current (voltage), which we explain by weakening the action of competing mechanisms of — exciton and size quantization. We reported on the anomalous temperature dependence of photoluminescence as a specific manifestation of dimensional quantization in QD in the study [12].

4. Electronic transport

Since, according to the conditions of gapless semiconductors applications the, long-wave effects are used, which are manifested in relatively large quantum dots (> 10 nm), in which dimensional quantization practically does not work, studies known from the literature, for example, reviews [3–5], were carried out using conventional models of electron transport in bulk semiconductors with the corrections for nanosizes per band structure properties, statistics, and density of charge carriers states.

In the case of dimensional quantization, the most important specifics of the motion of the injected into QD electron are one-electron transport [13] and the manifestation of quasi-periodic oscillations of the coefficient of transmission through a nanoparticle with a change in the electron energy [11]. In our case, this is expressed in the appearance of features in the current-voltage characteristics (CVC) in the form of peak current surges.

We measured CVC on single QD using scanning probe microscopy method, developed and described in our studies [14,15]. Just before the measurements, quantum dots were freed from ligands by separating the precipitate by centrifugation and redispersion in hexane and deposited as an island monolayer on a glass substrate with a conductive ITO layer using Langmuir–Blodgett film technology [16]. A tungsten filament with an end etched by the original technology was used as a probe for measuring CVCs.

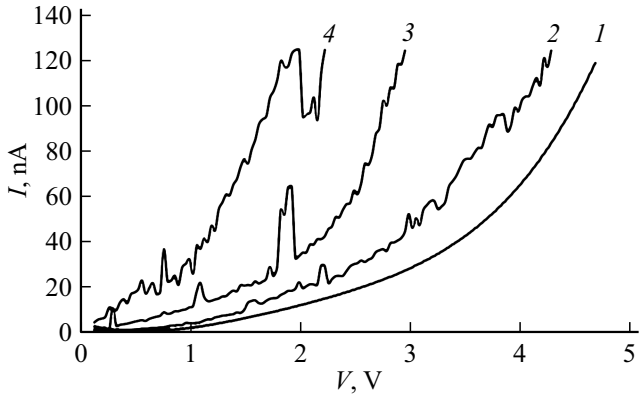

Figure 2. Typical CVCs QD-HgSe (see clarifications in the text).

Figure 2 shows typical CVCs of three types: without features (curve *1*), with weak (curve *2*) and strong (curves *3* and *4*) manifestations of specific features. The explanation of such observed phenomena is given in the below physical model of the dimensional quantization effect. From the total number of measured samples ~ 200 QD dots were identified: CVCs in Fig. 2, curve *1* — 10%, *2* — 60%, *3* and *4* — 30%. This breakdown is determined by the nature of the dimensional QD distribution (Fig. 1) and how each nanocrystal is located in the interelectrode gap during measurement.

CVCs of quantum dots without features, as shown in a number of our studies [13,15], are determined by the mechanisms of electron tunneling through a potential barrier (barrier tunneling) — $I \sim \exp[\alpha V]$ and Coulomb current limit — $I \sim V^{\beta}$. Statistical CVC analysis of the curve *1* type in Fig. 2 allowed to specify, that in our case, within the range of low voltages V, the current I is limited by the Coulomb limitation, and at high voltages by tunneling. The average statistical values of the parameters obtained in this case — $\alpha = 0.85$, $\beta = 1.89$ — correspond to the specified models [13,15].

The degree of dimensional quantization (QD) manifestation depends on the relation a and Λ. At $a > \Lambda$ QD does not manifest, and the CVC has practically no nonlinear distortions (curve *1* in Fig. 2). At $a \sim \Lambda$ QD manifests weakly, the CVC repeats the form of the previous case, but has quasi-periodic nonlinear distortions (curve *2* in Fig. 2). At $a < \Lambda$ QD manifests strongly, CVC has a form of curves *3* and *4* in Fig. 2. With an increase in the manifestation of QD, a significant increase in current is observed (curves in Fig. 2 shift to the left), which can be explained by the competitive predominance of dimensional quantization and resonant electron transport over the mechanisms of barrier tunneling and Coulomb limitation.

On all curves in Fig. 2 with the manifestations of features, small-profile quasi-periodic current oscillations are observed. They can be explained by Bloch oscillations, the appearance of which is theoretically possible, when an electron moves in

a quantum-dimensional structure [17]. However, in this case, the main obstacle for them is their short lifetime caused by the electron scattering on defects of the crystal lattice and phonons. In a quantum-size particle with dimensions of $a < \Lambda$ the electron moves in a ballistic and, perhaps, quasi-resonant manner, as if it „does not respond“ to the structural interference, and the „path“ of its motion in a three-dimensional QD is determined by quantum selection of the impulse in the Brillouin zone. These circumstances may be indicative of a real possibility of Bloch oscillations acting in the QD in the case of current flow or any other energy impacts on the electron. The energy increment $\Delta V \sim \Delta\tilde{E}$ of this oscillation in CVCs can be calculated by differentiating the formula (1) for the electron energy as a function of $\tilde{E}(a) - \Delta\tilde{E} \sim 0.7(a^3 m/m_)^{-1}\Delta a$. By assuming Δa is equal to QD nanocrystal lattice constant, approximate values $\Delta\tilde{E}$ can be calculated and compared with the data obtained from the curves in Fig. 2. Calculated and actual values $\Delta\tilde{E}$ — $\sim (0.05-0.1)$ V. In calculations, here and below, tabular data on semiconductor parameters are used: band gap — $E_g = 0.07$ eV; relative value of the effective electron mass — $m/m_0 = 0.045$; lattice syngony — cubic with a constant of 0.608 nm (https://xumuk.ru/encyklopedia/2/3935.html).

With applied voltage V from zero and above, the electron injected from the electrode to the QD is transferred to a steady resonant state of $n = 1$. The first zone of the feature $V_1 \sim \tilde{E}_1$ is manifested on the CVC. With further increase in V the electron is removed from this state by tunneling through the nanocrystal boundary and creates current until some next electron is transferred to the steady resonant state of $n = 2$. In this case, the second zone of the feature $V_2 \sim \tilde{E}_2$ is manifested on the CVC. The transition gap CVC will be defined by the ballistic tunneling of the electrons, which are successively flowing through the QD as a rectangular potential barrier. The probability of such tunneling can be calculated [18]: $\exp[-a[8m(\tilde{E}-V)]^{1/2}/h] \times \exp[-\gamma(n^2 - 3Va^2m/m_0)^{1/2}] \sim \exp[-\gamma C]$. Artificially introduced parameter $\gamma \geq 1$ takes into account the decrease in the probability of electron tunneling due to deviation of its wave vector from the electric field line depending on the electron velocity (energy) values, — the higher is the energy $\tilde{E}_{1,2}$, the lower is γ The results of CVC measurements will depend on the positioning of the QD monocrystal between electrodes in relation to the field lines. Figure 3 shows the dependence curves of $\ln I \sim C$ for three CVC regions of the curve *3* in Fig. 2. The values of the γ parameter are indicated in the figure caption.

Table 2. Statistical data on the current peaks on CVC

	$n=1$		$n=2$					$n=3$		
	1	2	3	4	5	6	7	8	9	10
$\tilde{E}_n$, eV	0.27	0.73	0.73	1.07	1.43	1.87	2.43	1.87	2.43	3.30
a, nm	5.4	3.3	6.5	5.4	4.7	4.1	3.6	4.6	5.4	4.6
p, %	5	9		13	15	16	17			25

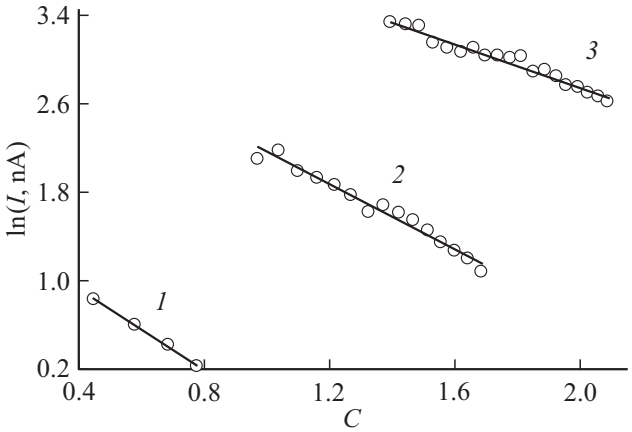

Figure 3. Characteristic $\ln I \sim C = (n^2 - 3Va^2m/m_0)^{1/2}$ QD-HgSe, $a = 5.5$ nm: *1* — $n = 1$, $\gamma = 1.8$; *2* — $n = 2$, $\gamma = 1.4$; *3* — $n = 3$, $\gamma = 1.0$.

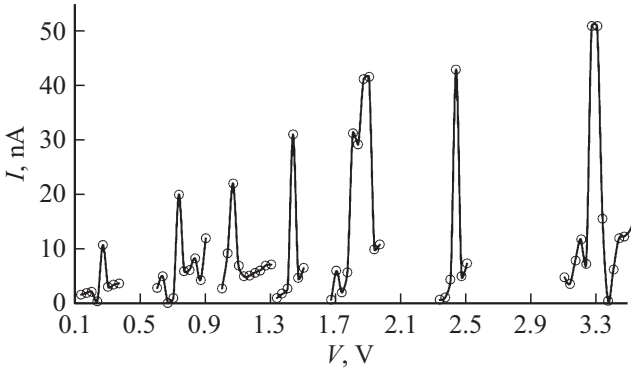

Figure 4. Current peaks in the CVC of a set of QD-HgSe samples.

Figure 4 shows typical CVC fragments of specific current peaks measured on a variety of samples. Table 2 shows statistical data on peak energies, their percentages p in the total amount, values of quantization size a calculated by formula (1) and peak energies. The data obtained in the next section are compared with the absorption spectra measurements.

5. Absorption spectra

The absorption spectra are used to judge the nature of optical transitions — interband and intraband, and their temperature dependences — the parameters of the band structure [3–5]. Absorption depending on QD-HgSe size was studied, for example, in the study [3], where it was shown, that within sizes up to ~ 10 nm, when QD-HgSe has a monocrystalline structure, intraband absorption occurs, the spectral distribution of which is subject to dimensional quantization. At large sizes (up to 30 nm) the structure becomes polycrystalline, and the absorption — interband with regularities similar to those of a large crystal.

Table 3. Absorption Spectra Data

Maxima on the curves in Fig. 4, 1/cm	7121–7213	5709–5863	4065–4328	2920	2360	1743	1465	1165
Quantum transition energy, meV	883–894	708–727	504–537	362	293	216	182	145
Transition types, as per Table 2	7–10	3–5	1–3	0–1	3–4			

Fig. 5 shows a typical absorption spectrum curve QD-HgSe measured by us, with maxima, which values are given in Table 3. On the basis of spectral maxima values the energies of quantum transitions are calculated and compared with the data in Table 2. The measurements were performed according to the method of our study [19] using a spectral complex based on an IR Fourier spectrometer IRAffinity-1 (Shimadzu Corp., Japan). The measurement results were processed in the Origin Pro 8 software package by Savitzky–Golay method using a second-order polynomial.

The most pronounced spectral maximum ($2920\,\mathrm{cm}^{-1}$, 362 meV) manifests as an interband transition — from the top of the valence band to the first resonant level $n = 1$. Other transitions, indicated in Table 3, are intraband interresonant transitions. Low-energy transitions (216, 182, 145 meV) cannot be identified as intraband interresonant ones. In our opinion, they can be classified as intraresonant, i.e. transitions within the energy limits of the current peaks Fig. 4. the absorption with low-energy transitions was also observed in studies [3,7] on relatively small QD-HgSe quantum dots (< 10 nm). Physically, the impact on an electron with a low-energy light quantum takes it out the resonant state and, accordingly, removes the peak on CVC.

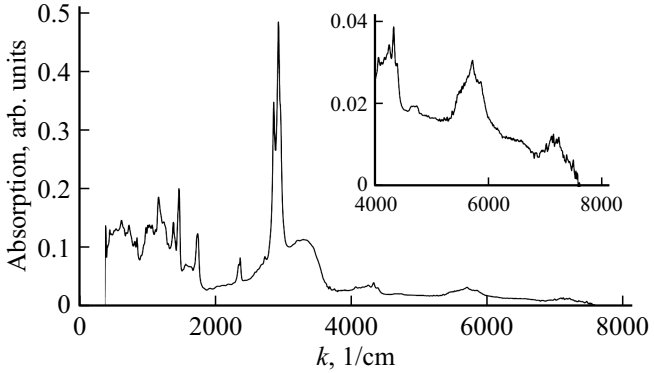

Figure 5. Typical absorption spectrum QD-HgSe.

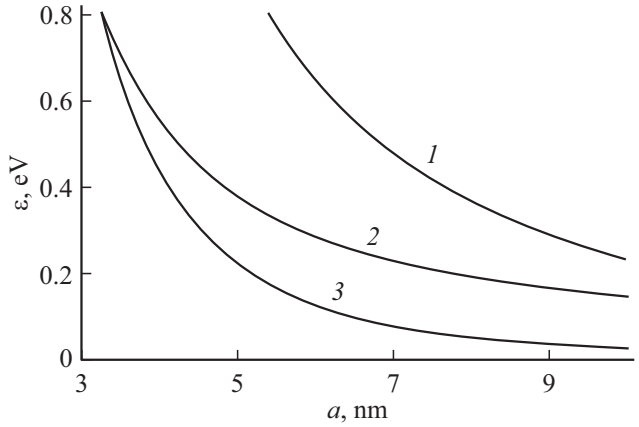

Figure 6. The calculated absorption energy minimum curves for energy transitions: *1* — interband, *2* — intraband interresonant, *3* — intraresonant.

Figure 6 shows the transition energy minimum dependences of the quantum dot size QD-HgSe calculated by formula (1) for three cases: interband (curve *1*), intraband interresonance (curve *2*) and intraresonance (curve *3*). The minimal energy values and, accordingly, the highest for the wavelength of absorbed IR-radiation: interband — 230 meV ($\sim 5\,\mu$m), intraband — 150 meV ($8\,\mu$m); intraresonant — 30 meV ($40\,\mu$m).

6. Conclusion

Mercury selenide nanocrystals (QD) were obtained by colloidal synthesis. For the synthesis, generalized literature data were used, on the basis of which the technology was developed under laboratory and production conditions. A precursor based on mercury oxide, which is much less toxic than commonly used organometallic compounds, was tested.

Volt-ampere characteristics of single quantum-dimensional (< 10 nm) QDs have features in the form of individual regular peaks and quasi-periodic current oscillations with its values up to 50 nA and voltage intervals (0.1–0.2) V. The observed features are explained in terms of dimensional quantization and Bloch pulses. Ten peak energy values distributed over three quantum (resonant) numbers were experimentally determined.

The absorption spectra in the range up to $25\,\mu$m have eight distinct peaks, including five — interband and intraband transitions and three — with energy (140–215) meV. Extremely low-energy peaks are identified by intraresonance transitions. The dependences of the minimum energy of absorption peaks on the quantum QD size are calculated and plotted. It is shown that, in principle, it is possible to have IR-photosensitivity within the wavelength range up to $40\,\mu$m.

Funding

This work was supported financially by the Russian Foundation for Basic Research No. 19-07-00595 (properties research) and 20-07-00307 (synthesis research).

Conflict of interest

The authors declare that they have no conflict of interest.

References

[1] S.B. Brichkin, V.F. Razumov. Uspekhi khimii, **85** (12), 1297 (2016) (in Russian).
[2] A.L. Efros, L.E. Brus. ACS Nano, **15**, 6192 (2021).
[3] C. Gréboval, A. Chu, N. Goubet, C. Livache, S. Ithurria. Chem. Rev., **121**, 3627 (2021).
[4] E. Lhuillier, P. Guyot-Sionnest. IEEE J. Select. Topics Quant. Electron., **23** (5), 6000208 (2017).
[5] M. Green, H. Mirzai. J. Mater. Chem. C, **6**, 5097 (2018).
[6] N.D. Zhukov, T.D. Smirnova, A.A. Khazanov, O.Yu. Tsvetkova, S.N. Shtykov. FTP, **55** (12), 1203 (2021) (in Russian).
[7] B. Martinez, C. Livache, L.D.M. Notemgnou. ACS Appl. Mater. Interfaces, **9** (41), 36173 (2017).
[8] X. Tang, G. Wu, K. Wai Chiu Lai. In: *Proc. 17th IEEE Int. Conf. on Nanotechnology* (Pittsburgh, IEEE, 2017) p. 641.
[9] S.E. Keuleyan, P. Guyot-Sionnest, C. Delerue, G. Allan. ACS Nano, **8** (8), 8676 (2014).
[10] M. Kristl, M. Drofenik. Ultrason. Sonochem., **15**, 695 (2008).
[11] V.P. Dragunov, I.G. Neizvestny, V.A. Gridchin, *Osnovy nanoelektroniki* (Logos, M., 2006) (in Russian).
[12] N.D. Zhukov, S.A. Sergeev, A.A. Khazanov, I.T. Yagudin. Pisma v ZhTF, **47** (22), 37 (2021) (in Russian).
[13] N.D. Zhukov, M.V. Gavrikov, D.V. Krylsky. Pisma ZhTF, **46** (17), 47 (2020) (in Russian).
[14] N.D. Zhukov, M.V. Gavrikov. Mezhdunar. nauch.-issled. zhurn., **8** (110), 19 (2021) (in Russian).
[15] N.D. Zhukov, M.V. Gavrikov, V.F. Kabanov, I.T. Yagudin. FTP, **55** (4), 319 (2021) (in Russian).
[16] J. Al-Alwani Ammar, A.S. Chumakov, M.V. Gavrikov, D.N. Bratashov, M.V. Pozharov, A.S. Kolesnikova, E.G. Glukhovskoy. Proc. Southwest State University. Engineering and Technologies, **9** (1), 56 (2019).
[17] R.A. Suris, I.A. Dmitriev. Uspekhi fiz. nauk, **173** (7), 769 (2003) (in Russian).
[18] L.L. Gol'din, G.I. Novikova, *Kvantovaya fizika. Vvodny kurs* (Institute of computer research, M., 2002) (in Russian).
[19] N.D. Zhukov, M.I. Shishkin, A.G. Rokakh. Pisma ZhTF, **44** (8), 102 (2018) (in Russian).